Applied Magnetic Resonance
https://doi.org/10.1007/s00723-023-01637-5

Applied
Magnetic Resonance

ORIGINAL PAPER

# Probing the "Dead-Time" in NMR by Combining Single Pulse and Solid Echo Experiments Followed by a Global Model Fit Analysis

**Eddy Walther Hansen**[1]

Received: 3 October 2023 / Revised: 26 November 2023 / Accepted: 1 December 2023


**Abstract**
The main question addressed in this work is how to probe the "effective dead-time" in an NMR instrument, i.e., the time needed to blank the receiver after an rf-pulse excitation to prevent damage to the receiver and to avoid any distortion of the NMR signal being sampled. The strategy is to design a suitable FID-model to fit the single pulse excitation (SPE) and solid echo pulse (SEPS) data (on solid Tricosane) using a Global model-fit analysis technique. The derived dead time is discussed with respect to sampling temperature (25–40 °C) and—in particular—with respect to the number of SEPS data involved in the Global fit analysis by applying the Bayesian Information Criterion (BIC) in combination with more traditional statistical analysis. It is concluded that the "effective dead time" can be determined within a standard error of less than 2.5%.

## 1 Introduction

A well-known problem that may arise when characterizing the phase composition and/or when probing the molecular dynamics in solid materials by $^{1}$H-FID NMR frequently originates from a too long "dead time, i.e., the time period during which the receiver is blanked—to avoid any distortion from the rf-pulse—typically appears when the dead-time approaches the same order of magnitude, or longer than the inherent spin–spin relaxation time ($T_2$) within the solid material [1–5]. In some cases it is possible to overcome the dead-time problem by applying a solid-echo pulse sequence (SEPS) or by combining single pulse excitation (SPE) and SEPS [6–11] experiments. This is reflected in publications by Nicot et al. [12] and Walsh et al. [13].

✉ Eddy Walther Hansen
e.w.hansen@kjemi.uio.no

[1] Department of Chemistry, University of Oslo, Blindern, P.O. Box 1033, 0315 Oslo, Norway

Published online: 27 December 2023

In this work *n-Tricosane* [$CH_3$–$(CH_2)_{21}$–$CH_3$] is chosen as a probe molecule which is shown to possess two different and distinct $T_2$ domains, within the range of 10 μs < $T_2$ < 30 μs. The purpose of the present work is to examine the robustness with which the dead-time can be determined by combining SPE and SEPS experiments by systematically varying the temperature and the inherent duration of the dead-time. The choice of a representative FID-model (characterized by $T_2$-relaxation times and shape parameters) is crucial when combining SPE and SEPS data in a Global fitting procedure. The results will be discussed with reference to a traditional statistical analysis combined with a BIC analysis. To the best of knowledge no such work has been noticed in the open literature.

## 2 Experimental Section

### 2.1 Materials

The probe material used in this study was *n-Tricosane* ($CH_3$-$(CH_2)_{21}$-$CH_3$) with a 99% purity (melting point of 321–323 K) from Aldrich (CAS Number 638-67-5).

### 2.2 Methods and Procedures

A commercial, low field TD NMR instrument (Model A4, Advanced Magnetic Resonance Ltd) operating at 0.50 Tesla was applied throughout in this work. All experiments were performed within the temperature range of 298–323 K, i.e. below the melting point of *n-Tricosane*. The temperature error was less than 0.3 K and the dwell time and the 90°-pulse length were set to 1 μs and 1.5 μs, respectively.

Each sample was packed into a 10 mm (outer diameter) NMR tube. In order to minimize the effect of rf-inhomogeneity and the inherent magnetic field heterogeneities, the NMR tube was filled up to a height of 10 mm, before placed into the most homogeneous part of the magnet. The static magnetic field heterogeneity was of the order of 1 kHz and the rf-inhomogeneity was less than 6% within the 1 $cm^3$ sample volume. The FID of bulk water was found to be approximately distortion-free only within an acquisition window up to about 150 microseconds.

Both Single Pulse Excitation (SPE) and Solid Echo Pulse (SEPS) experiments were acquired with 64 number of scans (NS) resulting in a maximum signal-to-noise (S/N) ratio of about 630 in the SPE experiments. Not surprisingly, the corresponding S/N-ratio in the SEPS experiments was smaller and decreased when increasing the inter-pulse delay D1 (see Fig. 1). For instance, the S/N-ratio decreased from 590 to about 360 when increasing D1 from 8 to 18 μs. Due to the Curie-effect, an additional decrease in the S/N-ratio is noted when increasing the temperature [14]. All FIDs were acquired on-resonance.

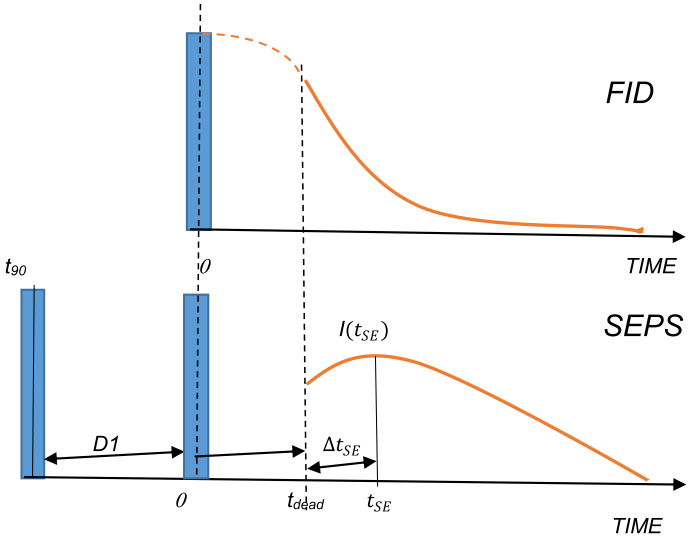


**Fig. 1** Schematic view of the relevant times and time periods in the SPE experiment (Top) and the SEPS-experiment (Bottom) where D1 is the time distance between the two successive 90° rf-pulses and $t_{90}$ is the length of the 90° rf-pulse, respectively. The dead time ($t_{dead}$) represents the blanking period of the receiver, i.e., the time duration from the mid-point of the detection pulse (t = 0) to the first sampling point ($t = t_{dead}$). The echo maximum in the SEPS experiment appears at time $t = t_{SE}$ where $\Delta t_{SE}$ defines the time period between the first observable data point ($t = t_{dead}$) and the echo maximum ($t = t_{SE}$)

### 2.3 Quantitative NMR

Quantitative NMR is based on a sampling of identical experiments with a time longer than 5*$T_1$ between successive experiments, with $T_1$ defining the longest spin–lattice relaxation time within the sample. Using an Inversion Recovery pulse sequence, the maximum $T_1$ of Tricosane was found to be less than 0.5 s (within the temperature range of 293–333 K). Hence, a repetition time of 3 s ensured quantitative sampling of both SPE and SEPS experiments. The analysis of all SPE data are based on an average of three individual SPE experiments.

### 2.4 Numerical Analysis

The SPE and SEPS data were analysed by a non-linear least squares (NLLS) technique combined with the Levenberg–Marquardt algorithm (Origin, version 2020, OriginLab Corporation, Northampton, MA, USA) and will be detailed later in this work.

### 2.5 Statistics and Bayesian Information Criterion (BIC)

In this work we will focus on two parameters, the dead time ($t_d$) and the initial FID signal intensity $I_{SPE}^{FID}(0)$ of the SPE experiment at time t = 0. These parameters will be derived by fitting relevant relaxation models to the observed SPE- and SEPS data, as detailed in Sects. 3.1 and 3.2. If not stated otherwise in the text, the average and standard deviation of each parameter are derived from Eqs. 1 and 2;

$$\overline{Y} = \sum_{i=1}^{N} y_i \left(\frac{1}{\sigma_i}\right) / \sum_{i=1}^{N} \frac{1}{\sigma_i} \tag{1}$$

$$\sigma(\overline{Y}) = \sqrt{\sum\nolimits_{i=1}^{N} \left(y_i - \overline{y}\right)^2 \left(\frac{1}{\sigma_i}\right)} / \sum_{i=1}^{N} \frac{1}{\sigma_i} \tag{2}$$

where $\sigma_i$ is the standard error in $y_i$ and $\overline{Y}$ signifies the weighted average of all $y_i$ with y representing the dead time $t_d$ or the FID signal intensity $I_{SPE}^{FID}(0)$ of the SPE experiment at time t = 0, respectively.

The choice of relaxation model is critical in the sense that it must result in a random error-distribution. Hence, in order to select the best model, a BIC number analysis is performed [15] in which the BIC number is defined by the Equation;;

$$BIC = nln\left(\frac{RSS}{n}\right) + kln(n) \tag{3}$$

where k is the number of model parameters and n is the number of data points. The residual sum of squares (RSS) represents the sum of squares between observed and model calculated data [16]. When comparing two different models, the model with the smaller BIC-number is the best if the difference (ΔBIC) between their respective BIC-numbers is larger than about two. Although the two models are not significantly different when ΔBIC < 2, the model with the least number of adjustable parameters is normally chosen—by convention.

### 2.6 Signal-to-Noise Ratio (SNR)

The signal-to-noise ratio (SNR) is defined by the equation; $SNR = I_0/\sigma_{FID,}$ in which $I_0$ and σ represent the observed maximum signal intensity and the standard deviation of the noise, respectively. The latter is defined by more than 50 data points and represents the signal free part of the experiment, i.e., the noise, only. Importantly, each FID was baseline corrected before model fitting.

## 3 Theory

### 3.1 Pulse Sequences

The two different pulse sequences (SPE and SEPS) applied in this work are illustrated on Fig. 1.

After applying a 90° detection pulse (t = 0), the receiver is blanked during the time $t_{dead}$ to prevent any damage of the electronics hardware and to avoid any distortion of the NMR signal. In low field NMR the dead time is typically 2–15 μs, and is expressed by Eq. (4):

$$t_{dead} = t_{dead}^{fix} + t_{dead}^{adjustable} \tag{4}$$

where the first term ($t_{dead}^{fix}$) is set by the manufacturer to avoid any damage of the electronics hardware. The second term ($t_{dead}^{adjustable}$) is controlled by the operator with the objective to remove any additional and minor distortion of the NMR signal being sampled. Finally, the time period between the two successive 90° rf-pulses in the SEPS experiment is defined by D1 and is set by the operator. Interestingly, it is shown both theoretically and experimentally that the observed echo maximum I($t_{SE}$) normally appears a time $t_{SE}$ different from D1 [8].

### 3.2 FID/SEPS Models

It is important to keep in mind that the SPE and the SEPS experiments both detect the free induction decay (FID). However, their respective FID appears at different times, as illustrated in Fig. 1. In the SPE experiment the first data point of the FID appears at time $t = t_{dead}$ while in the SEPS experiment the first FID data point occurs at the echo maximum, i.e., at time $t = t_{SE}$. Hence, In order to determine $t_{dead}$ a proper FID-model must be designed. In this work we adopt a generalized FID model which was recently applied successfully in the analyses of UHMWPE polymers [15] and is represented by Eq. (5).

$$I_{FID}(t) = I_C^0 \frac{\sin(\Delta\omega \cdot t)}{\Delta\omega \cdot t} E\mathrm{xp}\left[-\left(t/T_{2C}\right)^{d_C}\right] + I_A^0 \cdot E\mathrm{xp}\left[-\left(t/T_{2A}\right)^{d_A}\right] \tag{5}$$

where $I_C^0$ and $I_A^0$ represent the intensities of the ordered (crystalline) domains C and the less ordered (amorphous) domain A, respectively. $T_{2A}$ and $T_{2C}$ represent the relaxation times and $d_A$ ($0 < d_A < 2$) and $d_C$ ($1 < d_C \leq 2$) 1 define the shape factors of the respective FIDs. For $d_C$ and $d_A$ different from 1 or 2, both domains reflect structurally and dynamically heterogeneous domains with average relaxation time $<T_2>$, as defined by $\langle T_{2X} \rangle = \frac{T_{2X}}{d_X} \Gamma\left(d_X\right)$, where Γ represents the Gamma function and x = A or C [17]. The parameter Δω represents the static dipolar interaction term and is discussed in more details in Sect. 3.3. Other authors prefer to represent the FID by a finite sum of simple Gaussian (d = 2) and/or Exponential ($d = 1$) terms. This may, however, introduce additional adjustable parameters and thus affect the

robustness of the model, making it numerically less stable and to introduce significant inter-dependence between the adjustable parameters. Equation (5) will, however, be used to represent the FID throughout in this work.

### 3.2.1 Model A

Due to the presence of strong rf-pulses applied in both SPE and SEPS experiments, the initial part of the signal is blanked for a time $t_{dead.}$ Hence, the actual FID of the SPE experiment, denoted $I_{SPE}^{FID}(t)$ can be expressd by;

$$I_{SPE}^{FID}(t) = I_C^0 \frac{\sin\big((t+t_{dead})\cdot\Delta\omega\big)}{(t+t_{dead})\cdot\Delta\omega} Exp\Big[-\big((t+t_{dead})/T_{2C}\big)^{d_C}\Big] + I_A^0 \cdot Exp\Big[-\big((t+t_{dead})/T_{2A}\big)^{d_A}\Big] \tag{6a}$$

where the signal intensity at the first sampling point ($t=0$) is;

$$I_{SPE}^{FID}(t\to 0) = I_C^0 \frac{\sin\big((t_{dead}\cdot\Delta\omega\big)}{t_{dead}\cdot\Delta\omega} Exp\Big[-\big(t_{dead}/T_{2C}\big)^{d_C}\Big] + I_A^0 \cdot Exp\Big[-\big(t_{dead}/T_{2A}\big)^{d_A}\Big]$$

Likewise, by defining the time of the echo maximum in the SEPS experiment at $t=t_{SE}$ (see Fig. 1) the FID of the SEPS—denoted $I_{SEPS}^{FID}\big(t\geq t_{SE}\big)$—is represented by:

$$\begin{aligned} I_{SEPS}^{FID}\big(t\geq t_{SE}\big) &= I_C(D1)\cdot\frac{\sin\big(\Delta\omega\cdot(t-t_{SE}\big)}{\Delta\omega\cdot(t-t_{SE})} Exp\left[-\left(\frac{t-t_{SE}}{T_{2C}}\right)^{d_C}\right] \\ &+ I_A(D1)\cdot Exp\left[\left(\frac{t-t_{SE}}{T_{2A}}\right)^{d_A}\right] \end{aligned} \tag{6b}$$

It follows that the signal intensity at the echo maximum ($t\to t_{SE}$) becomes dependent on the inter-pulse distance D1 and reads;

$I_{SEPS}^{FID}\big(t\to t_{SE}\big) = I_C(D1) + I_A(D1)$. In summary, Eqs. (6a) and (6b) represent Model A.

### 3.2.2 Model B

A second relevant model with less adjustable parameters will also be considered in this work and is simply defined by the first term in Eq. (4), i.e., $I_{FID}(t) = I_C^0 \frac{\sin(\Delta\omega\cdot t)}{\Delta\omega\cdot t} Exp\left[-\left(\frac{t}{T\,2C}\right)^{d_C}\right]$.

Using the same arguments as in deriving Model A we obtain;

$$I_{SPE}^{FID}(t) = I_C^0 \frac{\sin\big((t+t_{dead})\cdot\Delta\omega\big)}{(t+t_{dead})\cdot\Delta\omega} Exp\Big[-\big((t+t_{dead})/T_{2C}\big)^{d_C}\Big] \tag{7a}$$

which implies that the signal intensity of the FID at time $t=0$ equals;

$$I_{SPE}^{FID}(t \to 0) = I_C^0 \frac{\sin\left(t_{dead} \cdot \Delta\omega\right)}{t_{dead} \cdot \Delta\omega} Exp\left[-\left(t_{dead}/T_{2C}\right)^{d_C}\right]$$

Likewise, we find that the FID of the SEPs experiment can be written;

$$I_{SEPS}^{FID}\left(t \geq t_{SE}\right) = I_C(D1) \cdot \frac{\sin\left(\Delta\omega \cdot (t - t_{SE})\right)}{\Delta\omega \cdot \left(t - t_{SE}\right)} Exp\left[-\left(\frac{t - t_{SE}}{T_{2C}}\right)^{d_C}\right] \quad (7b)$$

In particular, we note that that $I_{SEPS}^{FID}\left(t \to t_{SE}\right) = I_C(D1)$. Hence, Eqs. (7a) and (7b) represent Model B.

As the relaxation times and shape parameters of $I_{SPE}^{FID}$ and $I_{SEPS}^{FID}$ are identical, these parameters can be obtained by fitting Eq. (6b) [or Eq. (7b)] to the observed SEPS data. The dead time ($t_{dead}$) is subsequently determined from Eqs. (6a) [or Eq. (7a)].

In this work, a "Global fitting" procedure will be applied, in which the SPE and SEPS data are fitted simultaneously under the constraints that the relaxation times and shape parameters are identical in the two experiments. This approach has the advantage of improving the robustness of the numerical analysis by combining the SPE data with any number of SEPS data (different D1 times).

### 3.3 Distribution of $T_2$-Relaxation Times: Some Remarks

Pake was the first to derive an analytical expression for the line shape of interacting spin-1/2 nuclei, which inverse Fourier transform represents the corresponding FID. However, this inverse transformation results in a rather complex function, which is difficult to handle numerically [18]. Later, however, Abragam [14] suggested a much simpler, phenomenological expression for this "crystalline" FID-component, which is simply referred to as an "Abragamian" and is represented by the first term in Eq. (5). Despite its simplicity, it has been shown to give a good representation of the FID from other regular, crystalline lattices, as for instance semi-crystalline polyolefin.

As commented on by Hansen and co-workers in a recent paper [16] it is reasonable to ask why the shape parameter d may take a value different from two (2) or one (1). From basic theory, it follows that the (static) dipolar interaction term $\Delta\omega$ is proportional to the inverse cube of the distance $r$ between nuclei. Hence, the following equation results for PE; $\frac{\Delta\omega}{2\pi}(kHz) \approx 122\frac{1}{r(\text{Å})^3}$. Since the distance between a methylene proton and its neighbouring protons vary, it follows that the Abragamian must be modified accordingly, i.e.;

$$I_{FID}(t) = I_C \sum\nolimits_i f_i \frac{\sin\left(\frac{3}{2}\Delta\omega_i t\right)}{\left(\frac{3}{2}\Delta\omega_i t\right)} Exp\left[-\left(\frac{t}{T_{2C,i}}\right)^2\right] \quad (8a)$$

where $f_i$ represents the number-fraction of protons at the same distance from the reference proton (the factor 3/2 appears due to the spatial averaging of the dipolar interaction) as discussed by Wilhelm et al. [19]. Hence, Eq. (8a) can be identified as a distribution of Gaussian functions which can be represented by a much simpler function [20]:

$$I_{FID}(t) = I_C \mathrm{Exp}\left[-\left(\frac{t}{T_2}\right)^d\right] \tag{8b}$$

where $1 < \mathrm{d} < 2$ and $<T_2>$ defines the average $T_2$, according to:

$$< T_2 >= T_2 \frac{\Gamma(d)}{d} \tag{8c}$$

with $\Gamma$ representing the Gamma function. It follows that if $\Delta\omega_i$ approaches 0, Eq. (8a) can still be represented by Eq. (8b) ($\sum_i f_i$=1).

## 4 Notation Used to Uniquely Identify SPE/SEPS Data in This Work

As pointed out in Sect. 3.2 a Global model fitting procedure represents a more robust numerical approach in the analysis of the SPE and SEPS data. Hence, the notation SPE(t) and SEPS(t, D1) will be used to emphasize their dependence with respect to temperature (t) and inter-pulse distance (D1) between the two successive 90° rf-pulses in the SEPS experiment (see Fig. 1).

Moreover, since the SEPS experiment can be acquired with different D1 times, the Global fit analysis may involve more than a single SEPS. Hence, the notation SPE(t)/SEPS({D1}) is introduced in order to uniquely define all the data implemented in the Global fit analysis. A few examples will clarify this point.

***Example 1*** SPE(25)/SEPS(D1{8}) represents two data sets, one SPE data set and one SEPS data set acquired at t = 25 °C with D1 = 8 µs.

***Example 2*** SPE(25)/SEPS(D1{8–11}) represents five data sets, one SPE data set and four SEPS data sets acquired at t = 25 °C with D1 = 8 µs, 9 µs, 10 µs and 11 µs, respectively.

***Example 3*** SPE(31)/SEPS(D1{8–18}) represents 12 data sets, one SPE data set and 11 SEPS data sets acquired at t = 31 °C with D1 = 8 µs, 9 µs, 10 µs, …, 17 µs and 18 µs, respectively.

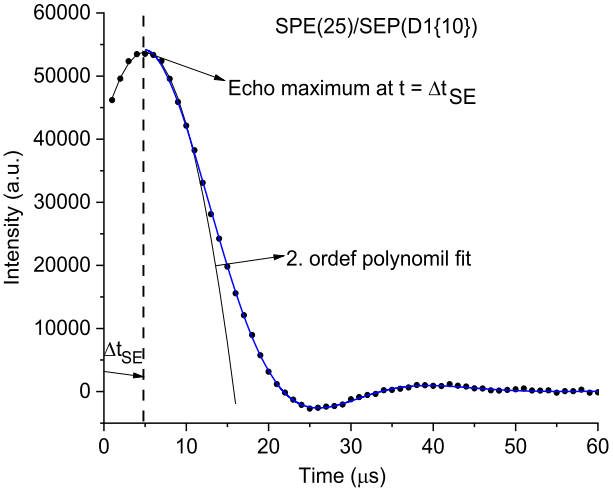


**Fig. 2** Observed echo curve E(t) (•) of the SPE(25)/SEPS(D1{10}) data as acquired at room temperature (25°C). The time t = 0 defines the end of the dead time ($t_{dead}$). The blue curve represents the FID ($I^{FID}_{SEPS}(t)$) and is derived from the procedure presented above, i.e.; $I^{FID}_{SEPS}\left(t - \Delta t_{SE}\right) = \mathrm{E(t)}$ where $\Delta t_{SE}$ represents the echo time relative to the first sampling point (t = 0)

## 5 Results and Discussion

### 5.1 How to Identify the FID Within a SEPS Experiment

To identify the FID—denoted $I^{FID}_{SEPS}$ (Sect. 3.2 and Fig. 1)—from the echo envelope $E(t)$ of a SEPS experiment the following procedure is applied;

(a) Set the time of the first observable data point in the SPE- and SEPS experiments to zero (0).
(b) Determine the time ($t_{SE}$) at the echo maximum of $E(t)$ by fitting a second order polynomial to the 6–8 data points around the echo maximum (solid black curve in Fig. 2).
(c) The final step is to note that for time $t \geq \Delta t_{SE}$ the FID can be expressed by $I^{FID}_{SEPS}\left(t - \Delta t_{SE}\right) = \mathrm{E(t)}$.

Hence, for $\Delta t_{SE} = 4.95$ μs (Fig. 2), it follows that: $I^{FID}_{SEPS}(0.05) = \mathrm{E(5)}$, $I^{FID}_{SEPS}(1.05) = \mathrm{E(5)}$ and $I^{FID}_{SEPS}(2.05) = \mathrm{E(6)}$ and so forth. In short, the above procedure is simply equivalent toa time-shift of the observed echo envelope E(t) by time—$t_{SE}$.

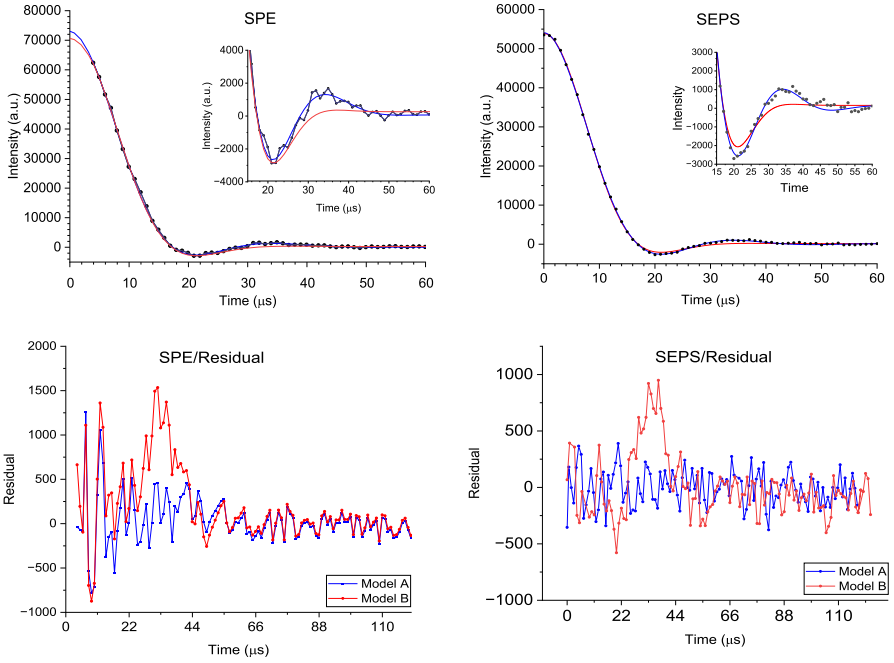


**Fig. 3** Top) Observed (•) and model-fitted $I_{SPE}^{FID}(t)$ FIDs, as obtained by Global fits of Model A (—) and Model B (—) to the SPE(25)/*SEPS*(*D1*{*10*}) data. The smaller figures represent vertical expansions of the respective FIDa. Bottom) Residuals (difference between observed and model fitted data) with respect to Model A (—) and Model B (—). All measurements were performed at 25°C

**Table 1** BIC numbers [Eq. (3)] calculated for the *SPE*(*25*)/*SEPS*(*D1*{*10*})-data with respect to Models A, B and C

| Model | n[)] | *k* | BIC |
|---|---|---|---|
| Model A (no parameter constraints) | 628 | 20 | 6802 |
| Model C (equal to Model A with $d_C$ fixed (=2) | 628 | 19 | 6860 |
| Model B (equal to Model A with $I_A(D1)$ fixed (=0) | 628 | 13 | 7378 |

The Residual Sum of Squares (RSS) was derived from the Global model fit for each model

## 5.2 Global Fit Analysis as Exemplified by the SPE(25)/SEPS(D1{10}) Data

In this Section the application of the Global fit analysis technique is demonstrated by fitting simultaneously two model equations, Eqs. (6a)/(6b) (Model A) and Eqs. (7a)/(7b) (Model B) to the SPE(25)/SEPS(D1{10}) data, which are composed of two distinct and different data sets, one SPE data set and one SEPS data set with D1 = 10 μs. This analysis procedure can be applied to any number of SPE and SEPS data and for any value of D1 and will be discussed in later sections.

According to the procedure outlined in Sect. 3.2, the results of the Global model fit analysis is illustrated in Fig. 3 where the observed FIDs are represented

by black dots (•). The blue and red curves represent Global model fits with respect to Model A and Model B, respectively. The residual curves are plotted in Fig. 3 (Bottom) and reveal a random error distribution with respect to Model A (—) and a slightly non-random error distribution with respect to Model B (—) suggesting that Model A is better than Model B. Actually, this statement was confirmed quantitatively by a BIC-number analysis in which the difference between the BIC-numbers of Models A and Model B was found to be larger than 500 (Table 1). Since it is generally accepted that a difference between two BIC numbers larger than about 2 represents a significant difference, we conclude that Model A is a much better Model representation than Model B [8].

A third model (Model C) which is frequently applied in the literature was also implemented in the analysis and differs from Model A by $d_C$ being fixed (=2). The results of the analysis are shown in Table 1.

Hence, based on the derived BIC numbers (Table 1) we conclude that Model A is statistically a significantly better model than Models B and C. Model A is thus the only model applied in the rest of this work.

### 5.3 Global Fit Analysis of SPE/SEPS Data Versus Inter-pulse Timing (D1) at Room Temperature (25 °C)

A corresponding Global fit analysis—as presented and discussed in the previous section (with D1 = 10 µs)—was performed on two other data sets; SPE(25)/SEPS(D1{$t_i$}) with $t_i$ (=D1) = 8, 9, 11, 12, …, 17, 18 µs and SPE(25)/SEPS(D1{8–11}). The observed FIDs (red and black dots) together with the corresponding Global model-fitted FIDs [$I_{SPE}^{FID}$ (—) and $I_{SEPS}^{FID}$) (—)] are shown in Fig. 4a, b. The numerical data derived by the Global model-fit analysis are summarized in Table 2.

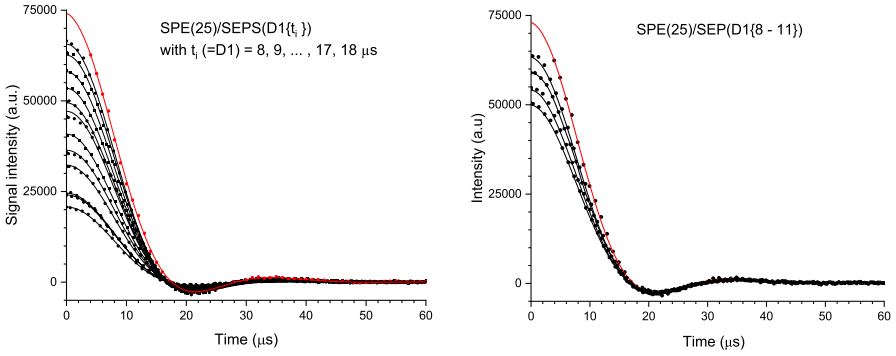


**Fig. 4** Observed FIDs from SPE (•)/SEPS (•) experiments of Tricosane at room temperature (25 °C). The red (—) and black (—) curves were obtained by a Global fit of Model A to the observed SPE(25)/SEPS(D1{$t_i$}) with $t_i$ (=D1) = 8, 9, 11, 12, …, 17, 18 µs (Left) and SPE(25)/SEPS(D1{8–11}) (Right). The solid curves represent the Global model fitted curves SPE [—; Eq. (6a)] and SEPS [—; Eq. (6b)]. See Sect. 3.2 for details

**Table 2** Dead time ($t_d$) and FID-intensity $I_{SPE}^{FID}(0)$ at time t = 0, as obtained by a Global Model fit analysis to the SPE/SEPS data; SPE(25)/SEPS(D1{$t_i$}) with D1 = 8, 9,…, 17, 18 µs, SPE(25)/SEPS(D1{8–11}) and SPE(25)/SEPS(D1{8–18})

| Data | D1 (µs) | $t_{dead}$ (µs) | $\Delta t_{SE}$[a] (µs) | $t_{SE}$[b] (µs) | $I_{SPE}^{FID}(0)$ (*a.u*) |
|---|---|---|---|---|---|
| SPE(25)/SEPS(D1{8}) | 8 | 3.88 ± 0.15 | 3.72 | 7.6 | $7.32\times10^4$ |
| SPE(25)/SEPS(D1{9}) | 9 | 3.90 ± 0.14 | 4.30 | 8.2 | $7.26\times10^4$ |
| SPE(25)/SEPS(D1{10}) | 10 | 3.86 ± 0.10 | 5.00 | 8.9 | $7.29\times10^4$ |
| SPE(25)/SEPS(D1{11}) | 11 | 4.16 ± 0.07 | 5.64 | 9.8 | $7.48\times10^4$ |
| SPE(25)/SEPS(D1{12}) | 12 | 4.34 ± 0.08 | 5.66 | 10.0 | $7.26\times10^4$ |
| SPE(25)/SEPS(D1{13}) | 13 | 4.16 ± 0.14 | 6.94 | 11.1 | $7.30\times10^4$ |
| SPE(25)/SEPS(D1{14}) | 14 | 4.31 ± 0.17 | 7.69 | 12.0 | $7.33\times10^4$ |
| SPE(25)/SEPS(D1{15}) | 15 | 4.05 ± 0.10 | 8.65 | 12.7 | $7.35\times10^4$ |
| SPE(25)/SEPS(D1{16}) | 16 | 4.21 ± 0.14 | 10.09 | 14.3 | $7.37\times10^4$ |
| SPE(25)/*SEPS*(D1{17}) | 17 | 4.00 ± 0.16 | 10.30 | 14.3 | $7.40\times10^4$ |
| SPE(25)/SEPS(D1{18}) | 18 | 4.11 ± 0.10 | 11.00 | 15.1 | $7.32\times10^4$ |
| SPE(25)/SEPS(D1{$t_i$}); $t_i$ = 8, …, 18 µs | Average[c] | 4.10 ± 0.16 | | | $(7.36\pm0.12)\times10^4$ |
| SPE(25)/SEPS(D1{8–11}) | Average[d] | 3.99 ± 0.10 | | | $(7.34\pm0.10)\times10^4$ |
| SPE(25)/SEPS(D1{8–18}) | Average[d] | 4.03 + 0.07 | | | $(7.40+0.10)\times10^4$ |

$\Delta t_{SE}$ (see Figs. 1 or 2) was derived by a 2. order polynomial fit, as illustrated in Fig. 2, with $t_{SE}(=\Delta t_{SE}+t_{dead})$ representing the time at the echo maximum. All measurements were performed at 25 °C

[a]See Fig. 2

[b]$t_{SE}=\Delta t_{SE}+t_{dead}$

[c]Derived by Eqs. (1) and (2)

[d]Derived by a Global fit analysis

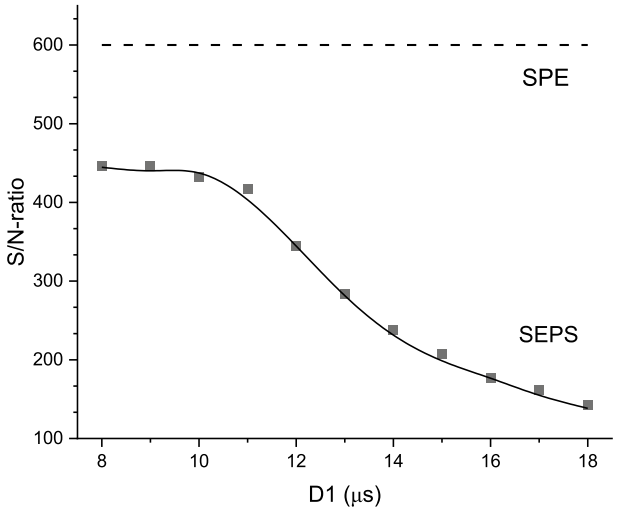


**Fig. 5** S/N-ratio in SPE- and SEPS experiments versus inter-pulse time D1

We notice that the observed echo times ($t_{SE}$) are different from the corresponding inter-pulse times (D1) and thoroughly discussed already in the 60'ties [8].

Importantly, a BIC number analysis (not shown) performed on all the data in Table 2 gives support to the conclusion that Model A is the better model with a weighted average dead time equal to $\overline{t_d} = (4.03 \pm 0.04)$ µs. Also, the narrow spread in the derived FID intensities $I_{SPE}^{FID}(0)$ versus D1, of less than 1.5%, suggests that the Global fit analysis technique is not restricted to only the shortest applied D1 time.

If adding extra SEPSs data in in the Global fit analysis a more robust model fitt is expected. However, this is not always the case, as recognized by the decrease in S/N-ratio of the SEPS experiment with increasing D1 (Fig. 5). For instance, the S/N-ratio is relatively constant for D1 equal to 8–11 µs, but decreases abruptly by more than 20% when D1 increases from 11 to 12 µs. A further increase in D1 to 14 µs, 16 µs and 18 µs reduces the S/N-ratio by approximately 50%, 60% and 70%, respectively.

Another parameter which affects the robustness of the model-fitting analysis relates to the ratio f between the total number of data points divided by the overall number of adjustable (model) parameters. For instance, if $I_{SPE}^{FID}$ and $I_{SEPS}^{FID}$ both contain N data points and the SPE- and SEPS models are defined by 8 and 7 adjustable parameters, respectively (see Sect. 3.2; Model A) we realize that a system composed of one SPE and n SEPS data will be characterized by $f = (n+1)\cdot N/(8+2n)$. Hence, we conclude that the robustness will improve asymptotically with increasing n ($f = 0.20$ for $n = 1$, $f = 0.31$ for $n = 4$ and $f = 0.44$ for $n = 18$) until f reaches an asymptotic value equal to 0.5 as n increases to infinity. However, increasing f implies an increasing number (n) of SEPS experiments, whcich in turn leads to an overall increase in the total experimental time. Hence, a compromise between n and the overall experimental time must be found. Based on experience we have chose $n = 4$ (D1 = 8, 9, 10 and 11 µs) in the rest of this work.

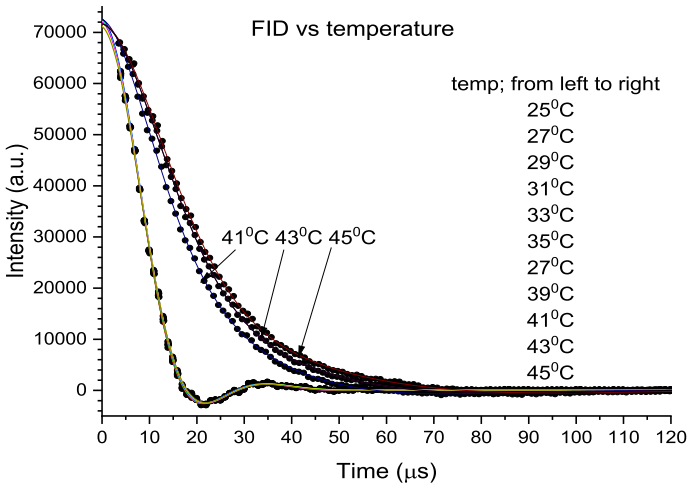


**Fig. 6** Observed (•) and model calculated ($I_{SPE}^{FID}(t)$;—) versus temperature. See text for further details

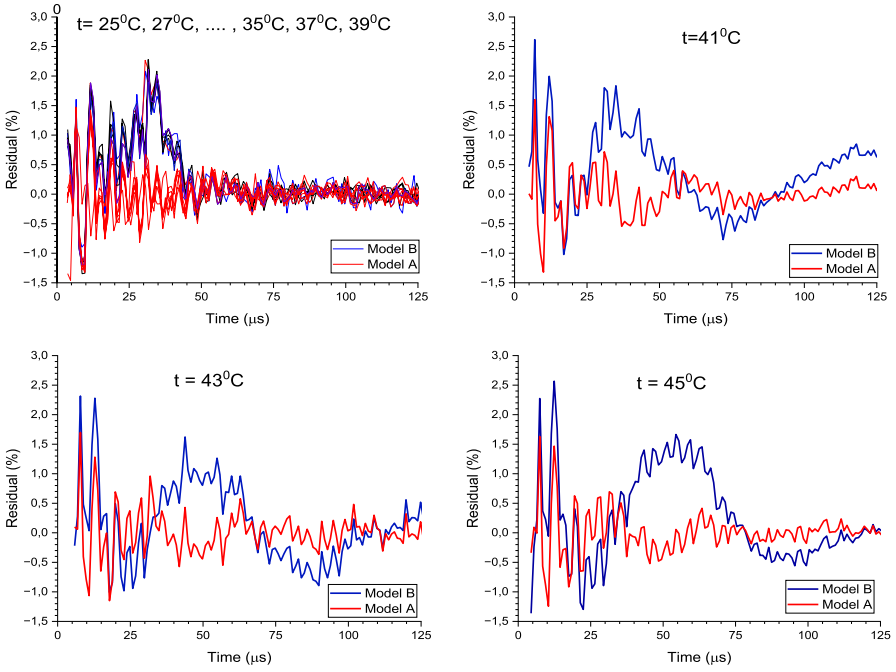


**Fig. 7** Residual curves of $I_{SPE}^{FID}(t)$ as derived from a global fit analysis of Model A (—) and Model B (—) to the observed *SPE(t)/SEPS(D1{8–11})* *data* within the temperature range 25–45 °C

Allthough the numerical values derived for the static dipolar interaction term Δω, the relaxation times and the shape parameters are of no concern in this work we still present the numerical values obtained from one data set; "SPE(25)/SEPS(D1{8–11})" to give the reader an idea of their dimension, i.e.; $T_{2A} = 11$ μs, $T_{2B} = 27$ μs, $d_A = 1.9$, $d_B = 1.5$, $\Delta\omega = 0.2149$ $s^{-1}$ and $I_A/I_B = 1.2$

**Table 3** Model derived dead time ($t_d$) and initial FID-intensity $I_{SPE}^{FID}(0)$ versus temperatures

| Temp/(°C) | $t_d$/(μs) | $I_{SPE}^{FID}(0)$ |
|---|---|---|
| 25.0 | 3.99 ± 0.09 | $7.32 \times 10^4$ |
| 27.0 | 3.84 ± 0.06 | $7.21 \times 10^4$ |
| 29.0 | 3.80 ± 0.07 | $7.19 \times 10^4$ |
| 31.0 | 4.07 ± 0.10 | $7.23 \times 10^4$ |
| 33.0 | 3.97 ± 0.09 | $7.22 \times 10^4$ |
| 35.0 | 3.84 ± 0.09 | $7.16 \times 10^4$ |
| 37.0 | 3.89 + 0.07 | $7.12 \times 10^4$ |
| 39.0 | 3.78 ± 0.07 | $7.05 \times 10^4$ |
| Average | 3.89 ± 0.09[a] | – |

[a]Derived by Eqs. (1) and (2)

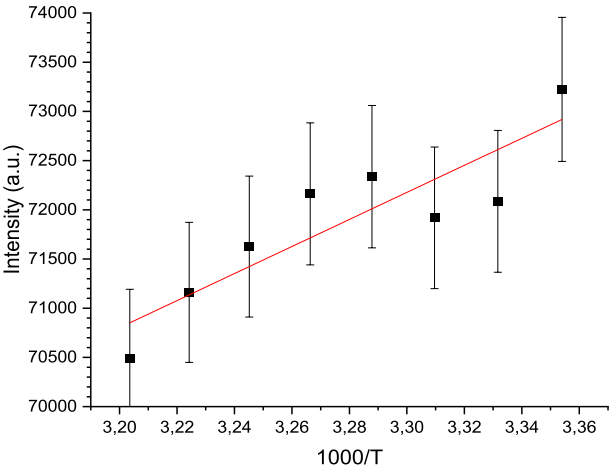


**Fig. 8** Signal intensity of $I_{SPE}^{FID}(0)$ versus 1000/T where T represents the absolute temperature. The red line represents a best linear fit to the Curie law, i.e.; $I_{SPE}^{FID}(0;T)) = k \cdot 1000/T$ where k is a constant [14]. The error bars represent a 1% relative standard error

### 5.4 Dead Time Derived from a Global Model Fitting to SPE/SEPS Data Versus Temperature

Figure 6 shows the observed and global modelled FIDs $\left(I_{SPE}^{FID}(t)\right)$ versus temperature and reveal an abrupt and significant change in line shape between 39 and 41 °C and is assigned to a dynamic transition taking place within this temperature range. However, since this transition is of minor importance in this work it we will not be pursued any further [21, 22]. A more critical question relates to whether Model A (and/or Model B) represents a reliable presentation of the SPE/SEPS data within the temperature range investigated.

Considering the residual curves (Fig. 7), i.e., the difference between observed and calculated $I_{SPE}^{FID}(t)$ versus temperature we conclude that Model A represents a better model as compared to Model B. However, at temperatures higher than 40 °C the residual curves—derived from Model A—start to reveal some slight non-random behaviour (oscillation) as well, indicating that Model A does not give a proper quantitative representation of the $I_{SPE}^{FID}(t)$. Hence, the data obtained above 41 °C are all excluded from further discussion.

The dead time and FID intensity $I_{SPE}^{FID}(0)$ derived from the *SPE(t)/SEPS(D1{8–11})* *data* by a Global fit to Model A at temperatures t = 25C, 27C, 29C, 31C, 33C, 35C, 37C and 39C are summarized in Table 3 (See Sect. 3.2 for further details)**.**

The relative standard error in $I_{SPE}^{FID}(0)$ was about 1% (see Sect. 4.2). Figure 8 reveals a small but significant increase in $I_{SPE}^{FID}(t)$ against the inverse absolute temperature (1000/T) which is expected according to the Curie law [14]. The red curve represents a best linear fit to the observed data,

The dead time ($t_0$) versus temperature (Table 3) is plotted in Fig. 8 and results in a weight-average dead time $t_d = (3.89 + 0.09)$ µs (red curves). From the results

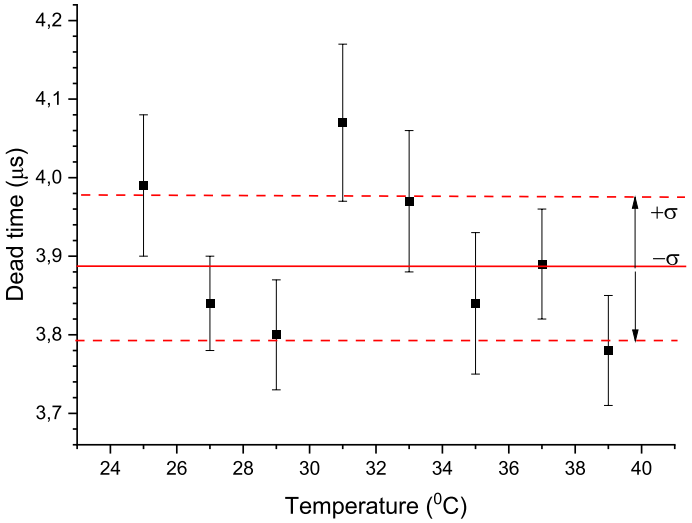


**Fig. 9** Dead time (•) and corresponding standard error (vertical ines) versus temperature. The red/solid line (—) represents the average value of all 8 data points with a standard error (±σ) as represented by the horizontal red/dashed lines (.– – –)

**Table 4** The number of initial data points removed from the original SPE/SEPS data are shown in column 1

| n | Notation SPE(25;n)/SEPS((D1{8–11}) | $t_d^{theory}(n)$(µs) | $t_d^{exp}(n)$ (µs) | $I_{SPE}^{FID}(0)$ (au) |
|---|---|---|---|---|
| 0 | SPE(25;0)/SEPS(D1{8–11}) | $d_0$ | $3.99 \pm 0.10$ | $7.33 \times 10^4$ |
| 1 | SPE(25;1)/SEPS(D1{8–11}) | $d_0+1$ | $4.80 \pm 0.13$ | $7.33 \times 10^4$ |
| 2 | SPE(25;2)/SEPS(D1{8–11}) | $d_0+2$ | $5.92 \pm 0.08$ | $7.37 \times 10^4$ |
| 3 | SPE(25;3)/SEPS(D1{8–11}) | $d_0+3$ | $6.90 \pm 0.08$ | $7.39 \times 10^4$ |
| 4 | SPE(25;4)/SEPS(D1{9–12}) | $d_0+4$ | $7.84 \pm 0.18$ | $7.30 \times 10^4$ |
| 5 | SPE(25;5)/SEPS(D1{10–13}) | $d_0+5$ | $8.76 \pm 0.11$ | $6.96 \times 10^4$ |
| 6 | SPE(25;6)/SEPS(D1{12–15}) | $d_0+6$ | $9.86 \pm 0.11$ | $7.18 \times 10^4$ |
| Average | | | | $(7.31 \pm 0.19) \times 10^4$ |

The assignment of the "mimicked" or "synthetic" SPE/SEPS data are shown in column 2 with the theoretically derived dead time shown in column 3. The dead time $t_{dead}^{exp}(n)$ and the initial signal intensity $I_{SPE}^{FID}(0)$ in columns 4 and 5 were derived from a Global fit analysis (using Model A), respectively

obtained in this work we conclude that by combining SPE and SEPS data (on Tricosane) in a Global model fit analysis, the dead time is probed within an error (standard error) of less than 2%.

We finally emphasize that the contribution $t_{dead}^{adjustable}$ to the overall dead time [Eq. (4)], which is controlled by the operator of the NMR instrument, was fixed at 2.0 µs throughout in this work, implying that the second contribution $t_{dead}^{fix}$ to the dead time (as set by the manufacturer to prevent any damage to the receiver) equals $t_{dead}^{fix} = (1.89 \pm 0.09)$ µs (Fig. 9).

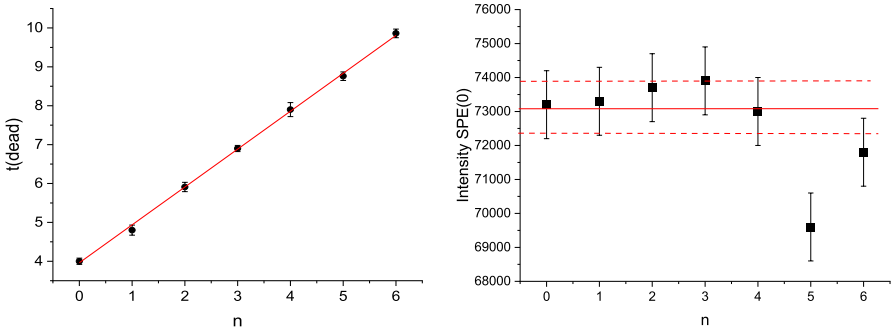


**Fig. 10** Observed (•) and model-fitted (—) dead time $t_{dead}$ (Left) and $I_{SPE}^{FID}$(•) versus n (Right). Based on a BIC-analysis the model-fitted curve is represented by $t_d(n) = d_0 + k_1 n$ with $d_0 = (3.96 \pm 0.04)$ μs and $k_1 = (0.974 \pm 0.012)$, respectively. See text for farther details

### 5.5 Dead Time Derived from SPE/SEPS Data After Removing Successively a Finite Number of Initial Data Points

By designing and applying a proper FID model (Model A) to fit the experimental SPE/SEPS data by a Global fit analysis a dead time $t_d$ $(=3.89 \pm 0.09)$ μs was derived. Importantly, since the time between successive data points equals 1 μs (dwell time), we are able to "mimic"SPE/SEPS data derived from any pre-selected dead time $t_d(n) = t_d + n$ by simply removing the n first data points successively from the original SPE/SEPS data. One point of concern, however, is that when removing data points from the original SEPS experiment one has to ensure that $t_{dead}^{theory}(n) \leq t_{SE}$ in order to obtain a reliable SEPS curve from the Global fit analysis! The actual SPE/SEPS data sets applied in the Global fit analysis are illustrated in column 2 of Table 4.

The observed dead time $t_{dead}^{exp}$(•) and $I_{SPE}^{FID}$(•) are plotted against n and shown in Fig. 10 (left and right) where the red line represents a model fitted curve which will be discussed next.

Keeping in mind that Model A is composed of two independent components with different relaxation times ($T_2$) and different shape parameters, the $t_{deas}^{exp}(n)$ may differ from $t_{dead}^{theory}(n) = d_0 + n$. Hence, two additional and plausible models (b) and (c) are implemented in the analysis and their corresponding BIC numbers shown in Table 5. In order to decide which model is statistically better, a BIC-number analysis [15, 16] was performed and the results summarized in Table 5.

**Table 5** BIC-number for model (a), (b) and (c)

| Model | BIC |
|---|---|
| $t_{dead}^{(a)}(n) = d_0 + n$ | −2.18 |
| $t_{dead}^{(b)}(n) = d_0 + k_1 n$ | −4.59 |
| $t_{dead}^{(c)}(n) = d_0 + k_2 n + k_3 n^2$ | −3.22 |

From the BIC-analysis [16] we conclude that Model (b) is slightly better than Models (a) and (c). A linear regression analysis shows that $d_0 = (3.96 \pm 0.04)$ µs with $k_1 = (0.974 \pm 0.012)$, respectively.

The results show that $k_1$ deviates by less than 3% from its theoretical value of 1.00, suggesting that a systematic deviation between the observed and model derived dead times is small and barely observable, at least for D1 up to 10 µs.

## 6 Summary/Conclusion

The inherent dead time ($t_{dead}$) of and NMR probe has been explored by combining the FIDs acquired by a Single Pulse Excitation (SPE) experiment and a Solid Echo Pulse Sequence (SEPS). The analysis was based on fitting a generalized FID-model (Model A) to the observed FIDs by a simultaneous Global fitting approach in which the two model FIDs were represented by the equations;

$$I_{SPE}^{FID}(t) = I_C^0 \frac{\sin\left(\left(t + t_{dead}\right) \cdot \Delta\omega\right)}{\left(t + t_{dead}\right) \cdot \Delta\omega} Exp\left[-\left(\left(t + t_{dead}\right)/T_{2C}\right)^{d_C}\right] + I_A^0 \cdot Exp\left[-\left(\left(t + t_{dead}\right)/T_{2A}\right)^{d_A}\right]$$

$$I_{SEPS}^{FID}\left(t \geq t_{SE}\right) = I_C(D1) \cdot \frac{\sin\left(\Delta\omega \cdot \left(t - t_{SE}\right)\right)}{\Delta\omega \cdot \left(t - t_{SE}\right)} Exp\left[-\left(\frac{t - t_{SE}}{T_{2C}}\right)^{d_C}\right] + I_A(D1) \cdot Exp\left[\left(\frac{t - t_{SE}}{T_{2A}}\right)^{d_A}\right]$$

respectively, where $t_{SE}$ represents the time at the echo maximum and $I_C^0$ and $I_A^0$ represent the intensities of the two structurally and dynamically heterogeneous domains A and C with $T_{2A}$ and $T_{2C}$ representing the relaxation times and $\Delta\omega$, $d_A$ and $d_C$ ($0 < d_A < 2$ and $1 < d_C \leq 2$) defining the (static) dipolar interaction and the shape parameters of the FIDs, respectively. It is worth noticing that the relative signal intensities $I_C$ and $I_A$ in the SEPS experiment become dependent on the inter-pulse distance D1. Two additional models were also considered in which a) $d_C = 0$ (Model B) and b) $(I_A(D1) = I_A^0 = 0$ (Model C), respectively.

Only Model A resulted in a dead time that was constant and internally consistent with an error-distribution which was statistically random and independent on temperature and *D1*. The relative standard error $\sigma(t_d)$ was found to be less than 2%.

Finally, since the instrument was set up with a sampling rate of 1 point/µs it became possible to "mimic" SPE/SEPS data as a function of dead time by successively removing the n (=0, 1, 2, …, 5, 6) first data points from the observed SPE/SEPS data, before model-fitting. A Global model fit on each reduced data set (fixed n) revealed a dead time which increased linearly with increasing n according to the Equation; $t_{dead}(n) = d_0 + k \cdot n$ with $d_0 = (3.96 + 0.04)$µs and k = 0.974 ± 0.012. Hence, an estimate of the dead time was accessible up to a dead time of 10 µs with a standard error less than 2%.

**Acknowledgements** The author thanks the Department of Chemistry at the University of Oslo for all the resources to enable this work. The author has no relevant financial or non-financial interests to disclose.

**Author Contributions** Eddy Walther Hansen is a single author of this manuscript

**Funding** Open access funding provided by University of Oslo (incl Oslo University Hospital). The author is professor emeritus at Department of Chemistry, University of Oslo and thanks this institution for the resources to this work.

**Availability of Data and Materials** The data that support the findings of this study are available from the corresponding author upon reasonable request.

## Declarations

**Conflict of interest** The author has no relevant financial interests to disclose.

**Ethical Approval** The author has no relevant financial or non-financial interests to disclose.



## References

1. V.M. Litvinov, J.P. Penning, Phase composition and molcular mobility in nylon 6 fibers as studied by proton NMR transverse magnetization relaxation. Macromol. Chem. Phys. **205**, 1721–1734 (2004)
2. A. Maus, C. Hertlein, K. Saalwächter, A robust proton NMR method to invetigate hard/soft ratios, crystallinity, and component mobility in polymers. Macromol. Chem. Phys. **207**(13), 1150–1158 (2006)
3. V.M. Litvinov, EPDM/PP thermolastic vulcanizates as studied by proton nmr relaxation: phase composition, molecular mobility, network structure in the rubbery phase, and network heterogeneity. Macromolecules **39**(25), 8727–8741 (2006)
4. R.H.S. Garcia, J.G. Filgueiras, E.R. de Azevedo, L.A. Colnago, Power-optimized, time-reversal pulse sequence for a robust recovery of signals from rigid segments using time domain NMR. Molecules **27**, 566 (2022)
5. V. Litvinov, Y. Men, Time-domain NMR in polyolefin research. Polymer (2022). https://doi.org/10.1016/j.polymer.2022.125205
6. J.G. Powles, J.H. Strange, Zero time nuclear magnetic resonance transient in solids. Proc. Phys. Soc. **82**, 6–15 (1963)
7. P. Mansfield, Multiple-pulse nuclear magnetic resonance transients in solids. Phys. Rev. **137**(3A), A961–A974 (1965)
8. N.A. Sergeev, A.V. Sapiga, D.S. Ryabushkin, Shape of two-pulse NMR echoes in solids. Phys. Lett. A **137**(4–5), 210–212 (1989)
9. P. Bilski, N.A. Sergeev, J. Wasicki, Solid-echo in solids with molecular motions: effects of nonzero pulse widths. Appl. Magn. Reson. **18**, 115–126 (2000)
10. P. Bilski, N.A. Sergeev, J. Wasicki, Echoes in spin systems with dipolar interactions. Mol. Phys. **47**(15), 5163–5173 (2014)
11. D.E. Barnaal, I.J. Lowe, Measured nuclear magnetic resonance free-induction-decay shapes and moments for $F^{19}$ in $CaF_2$. Phys. Rev. **148**(1), 328–331 (1966)
12. B. Nicot, M. Fleury, J. Leblond, Measurement of short NMR relaxation times: effect of radio-frequency pulse length. C. R. Chim. **11**, 506–514 (2008)
13. D.O. Walsh, E. Grunewald, P. Turner, A. Hinnell, P. Ferre, Practical limitations and applications of short dead time surfaca NMR. Near Surf. Geophys. **9**, 103–111 (2011)
14. A. Abragam, *The Principles of Nuclear Magnetism* (Clarendon Press, London, 1961). ISBN, 019852014X, 9780198520146, p. 2

15. M. B. Priestley, in *Spectral Analysis and Time Series: Probability and Mathematical Statistics* (Academic Press, London, 1981), p. 7
16. E. Hansen, A. Hassani, Quantitative evaluation of phase distribution in UHMWPE as derived from a combined use of NMR FID analysis and monte carlos simulations. Appl. Magn. Res. **53**, 417–439 (2022). https://doi.org/10.1007/s00723-021-01456-613
17. M. Abramowitz, I.A. Stegun, "Gamma (Factorial) Function" and "Incomplete Gamma Function". §6.1 and 6.5 in *Handbook of Mathematical Functions with Formulas, Graphs, and Mathematical Tables, 9th printing* (Dover, New York, 1972), pp. 255–258 and 260–263
18. M. Goldman, L. Shen, Spin–spin relaxation in LaF3. Phys. Rev. **144**(1), 321 (1966)
19. V. Räntzsch, M. Haas, M.B. Ozen, K.-F. Ratzsch, K. Riazi, S. Kauffmann-Weiss, J.K. Palacios, A.J. Müller, L. Vittorias, G. Guthausen, M. Wilhelm, Polymer crystallinity and crystallization kinetics via benchtop 1H NMR relaxometry: revisited method, data analysis, and experiments on common polymers. Polymer **145**, 162–173 (2018)
20. E.W. Hansen, X. Gong, Q. Chen, Compressed exponential response function arising from a continuous distribution of gaussian decays-distribution characteristics. Macromol. Chem. Phys. **214**(7), 844–852 (2013)
21. H.G. Olf, A. Peterlin, NMR sudy of molecular Motion in orieted long-chain alkanes. III oriented n-C32H66. J. Polym. Sci. Part A-2 **8**, 791–797 (1970)
22. K. Kato, X-ray study of molcular motions in the rotator phases of normal tricosane. Polym. J. **48**, 253–258 (2016)